ISSN 0957-4484

NANOTECHNOLOGY

VOLUME 26 NUMBER 22 5 JUNE 2015

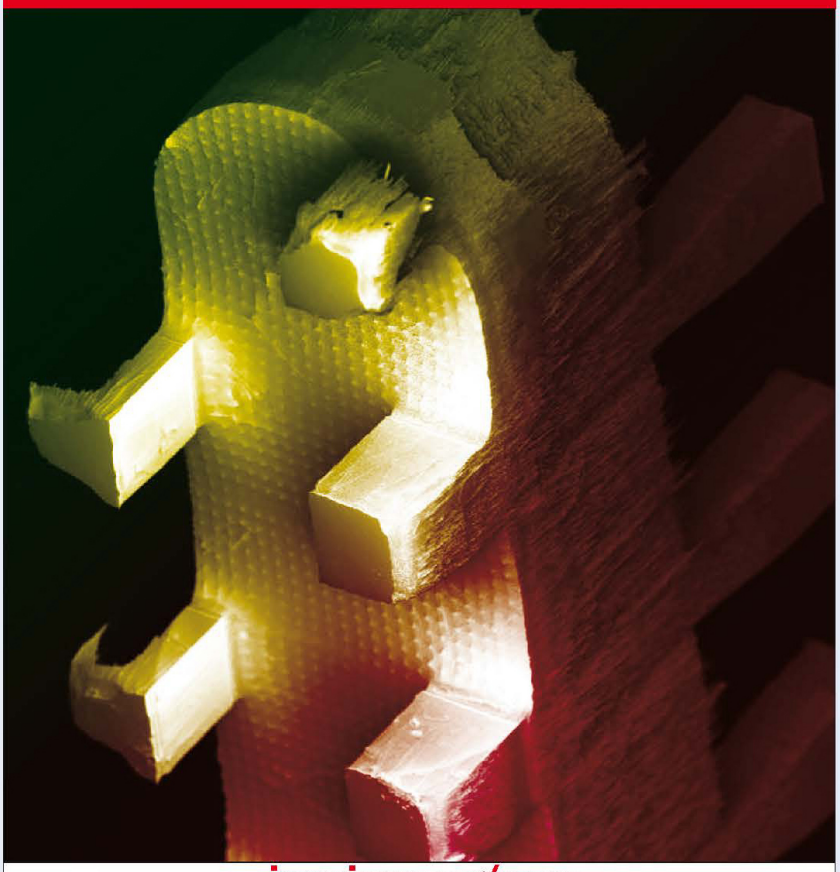

iopscience.org/nano

Featured article

Parallel nanomanufacturing via electrohydrodynamic jetting from microfabricated externally-fed emitter arrays

Philip J Ponce de Leon, Frances A Hill, Eric V Heubel and Luis F Velásquez-García

IOP Publishing

OPEN ACCESS
IOP Publishing
Nanotechnology

Nanotechnology **26** (2015) 225301 (10pp)
doi:10.1088/0957-4484/26/22/225301

Parallel nanomanufacturing via electrohydrodynamic jetting from microfabricated externally-fed emitter arrays

Philip J Ponce de Leon[1], Frances A Hill[2], Eric V Heubel[1] and Luis F Velásquez-García[2]

[1] Department of Mechanical Engineering, Massachusetts Institute of Technology, 77 Massachusetts Ave., Cambridge, MA 01239, USA
[2] Microsystems Technology Laboratories, Massachusetts Institute of Technology, 77 Massachusetts Ave., Cambridge, MA 01239, USA

E-mail: Velasquez@alum.mit.edu

Received 3 February 2015, revised 29 March 2015
Accepted for publication 10 April 2015
Published 11 May 2015

Abstract

We report the design, fabrication, and characterization of planar arrays of externally-fed silicon electrospinning emitters for high-throughput generation of polymer nanofibers. Arrays with as many as 225 emitters and with emitter density as large as 100 emitters cm^{-2} were characterized using a solution of dissolved PEO in water and ethanol. Devices with emitter density as high as 25 emitters cm^{-2} deposit uniform imprints comprising fibers with diameters on the order of a few hundred nanometers. Mass flux rates as high as 417 g hr^{-1} m^{-2} were measured, i.e., four times the reported production rate of the leading commercial free-surface electrospinning sources. Throughput increases with increasing array size at constant emitter density, suggesting the design can be scaled up with no loss of productivity. Devices with emitter density equal to 100 emitters cm^{-2} fail to generate fibers but uniformly generate electrosprayed droplets. For the arrays tested, the largest measured mass flux resulted from arrays with larger emitter separation operating at larger bias voltages, indicating the strong influence of electrical field enhancement on the performance of the devices. Incorporation of a ground electrode surrounding the array tips helps equalize the emitter field enhancement across the array as well as control the spread of the imprints over larger distances.

Keywords: electrospray, electrospinning, multiplexed nanofiber source, MEMS-enabled nanofabrication

(Some figures may appear in colour only in the online journal)

Introduction

Electrohydrodynamic jetting occurs when a strong electric field is applied to the free surface of a conductive liquid [1]; the process is capable of uniformly producing ion plumes, fine aerosol droplets, or continuous fibers with submicron diameters (i.e., nanofibers) depending on the properties of the liquid used and the ionization conditions [2–4]. Nanofabrication via electrohydrodynamic jetting has recently received attention as a promising candidate for the production of nanostructures because of its capability to create nano-thick films of high quality at lower temperature than standard semiconductor device fabrication [5]. A key advantage of electrospinning [6], i.e., the electrohydrodynamic jetting of nanofibers, over other fiber generation methods is its versatility in producing fibers of arbitrary length from a wide range of possible materials including polymers, metals, ceramics,

and semiconductors. Therefore, the applications of electrospun nanofibers are numerous. For example, dye-sensitized solar cells benefit from the reduction of grain boundaries associated with the one-dimensional structure of nanofibers, which improves charge conduction while allowing better infiltration of the viscous dye-sensitized gel due to the nanofiber mat's high porosity [7]. Also, the high surface-to-volume ratio of nanofiber mats makes them ideal scaffolds for catalyst dispersion in fuel cells or cell growth in tissue engineering [8]. In addition, the large surface-to-volume ratio and high porosity of electrospun nanofiber mats enable efficient interaction with fluid flow for applications such as ultracapacitors, biosensors, and separation membranes [4].

Electrospinning has traditionally been performed from the tip of a hollow syringe needle through which the liquid of interest is pumped at very low flow rates—on the order of a few μl min^{-1}. For most common polymer solutions, this translates to a mass production rate as low as 0.01 g hr^{-1}, which is very small compared to the mass production rate on the order of hundreds of grams per hour per spinner for mechanically drawn fibers [9–10]. This is not surprising because the mass throughput of a fiber spinner scales linearly with the draw rate and with the square of the fiber diameter; therefore, electrospun nanofibers with diameters <1000× smaller than those of conventional, mechanically drawn fibers exhibit a throughput that is <1000 000× smaller at identical draw rates. Increasing the draw rate only partially compensates for the large difference in diameter between the two kinds of fibers, as drawing a fiber supersonically can produce a shockwave [11]. This low throughput restricts the use of electrospun fibers to high-end products and research.

A promising alternative to greatly increase the throughput of an electrospinning source is to spin from many different points at the same time [12]. Several different approaches have been proposed to multiplex an electrospinning source; the most obvious, perhaps, is the use of multiple syringe needles in parallel [13]. Although this approach does increase throughput, it does not scale up well to large emitter densities. Other work has used a ferrofluid covered in polymer solution [14], where a large magnetic field triggers an instability in the ferrofluid that forms sharp spikes, which act as emission sites for fiber spinning. This method is simple but suffers from non-uniformity and offers little control over the positioning of the spikes. Some research has focused on spinning from a one-dimensional emission site (i.e., an edge) rather than a zero-dimensional emission site (i.e., a needle). For example, there are reports of electrospinning from a narrow, confined channel [15], from the edge of a bowl [16], and from a coil of wire [17]. This approach works but lacks control, and the emitter density does not scale up well. Another successful approach has been to electrospin fibers directly from the free surface of a liquid [18], eliminating the need for pumps or channels of any kind; however, this process can require voltages as high as 100 kV, lacks good repeatability, and exhibits inferior fiber uniformity.

Microengineered electrospinning sources have also been investigated as a way to achieve large production of nanofibers. Using batch microfabrication, arrays of emitters with large array size and high emitter density can be manufactured at low cost [19–21], which should result in low-cost, high-throughput production of nanofibers. For example, linear arrays of internally-fed electrospinning sources based on PDMS [22] and silicon microfluidics [23] have been reported. However, the miniaturization of a pressure-fed hydraulic network greatly increases the power requirements to pump the liquid (in an internal flow, the pressure gradient is inversely proportional to the fourth power of the inner diameter of the pipe). This increases the likelihood of clogging, especially when the working liquid is highly viscous and non-Newtonian. Also, spinning directly from microfluidic orifices coming out of a flat surface provides less electric field enhancement than needles; therefore, these emitters require a larger bias voltage to operate compared to a needle-like structure. Moreover, near-field electrospinning is a technique that employs significantly lower voltages applied over much smaller working distances in order to spin fibers in a more stable fashion [24, 25], introducing the possibility of precise fiber deposition. This work explores electrospinning from silicon-based, batch-fabricated two-dimensional arrays of externally-fed emitters as a potential technology to produce nanofibers in large quantities.

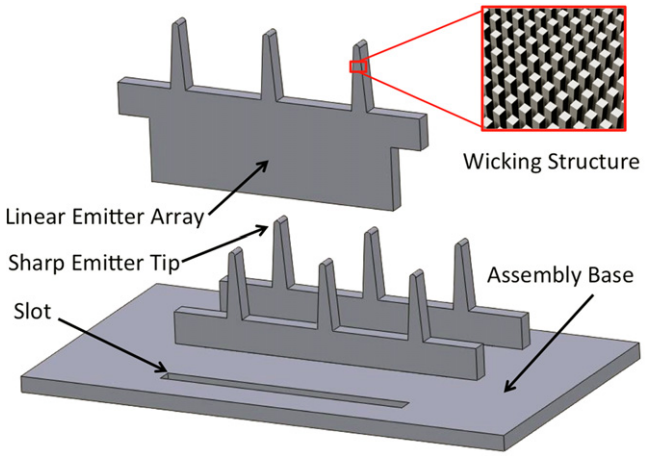

Figure 1. Schematic of the microengineered electrohydrodynamic emitter arrays used in this work. A series of monolithic linear arrays of emitters, i.e., blades, are assembled into a slotted base to form a planar array. The front and back surfaces of the emitter blades are covered by monolithic arrays of micropillars that act as a wicking structure.

Device design and fabrication

The proposed device architecture is a planar array of high-aspect-ratio, small-tip-diameter emitters with surfaces covered by an array of micropillars as a wicking structure that enables passive, surface tension-driven feed of liquid to the emission sites at the emitter tips (figure 1). The planar array is assembled from monolithic linear arrays of emitters, i.e., blades. The emitter blades are etched out of a silicon wafer using deep reactive-ion etching (DRIE) and are defined by three primary dimensions: the emitter length l_e, the emitter tip

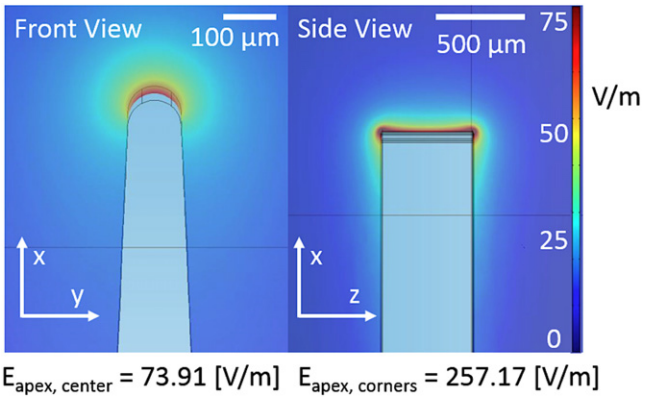

Figure 2. Cross-sections of a 3D simulation of the electric field generated by a DRIE-patterned emitter using the commercial software COMSOL: *x*–*y* cross-section passing through emitter midpoint (left), and *x*–*z* cross-section passing through emitter midpoint (right). The simulation was carried out for 1 V bias voltage between the emitter and a plate located 3 cm above the emitter tip.

radius R_{tip}, and the emitter spacing s. The micropillar structure is described by three other primary dimensions: the pillar height h, the pillar pitch p_M, and the pillar width d (the pillars have square cross-section). The dimensions were selected based on a study of the physics that describe the dynamics in the array, taking into consideration the fabrication capabilities we had available. On the one hand, emitters with larger length and smaller tip radius have greater electric field enhancement; on the other hand, emitters that are wider and shorter can transport a larger flowrate to the tip.

In terms of the capability of the emitters to concentrate the electrical field on their tips, it is highly desirable to have long and narrow emitters made from substrates with thickness on the order of the tip diameter to define a roughly symmetric, high aspect-ratio geometry. However, the microfabrication process used to pattern the emitters inherently generates sharp corners, which are the features that trigger the electrohydrodynamic jetting. DRIE etches long and narrow vertical trenches—similar to 'cookie-cutting' a sheet of dough; therefore, the 90° sidewalls define a very sharp edge that greatly increases the local electric field. An example of the electric field enhancement of the DRIE-cut emitters from 3D simulations using the commercial software COMSOL is shown in figure 2; the figure shows the 3D simulation results for one design in two perpendicular planes (*x*–*y* and *x*–*z*). The simulated emitter is 5 mm tall, 500 μm thick, has an *x*–*y* plane diameter equal to 100 μm, and has sidewalls that slope outward 5° from the vertical in the *x*–*y* plane. A 3 mm emitter spacing is simulated by setting periodic boundary conditions at a distance of 1.5 mm from the emitter axis in each of the four perpendicular directions. The emitter is set to 0 V and a 1 V potential is applied to a plate at a distance of 3 cm from the emitter tip; the simulation is iterated, refining the finite element mesh until the error of the solution is less than 1%. The simulation results suggest that the sharp corners at the front and back of the emitter (*x*–*z* plane) that result from DRIE etching provide the dominant field enhancement as compared to the relatively large radius of curvature in the perpendicular direction (*x*–*y* plane). The actual values of the field enhancement depend on the radius of curvature of the sharp edge, typically on the order of a micron, and the inherent roughness of DRIE sidewalls due to the alternation of passivation and etch steps, on the order of a fraction of a micron [26].

The characteristic length of relevance for the hydraulic design of the emitter is the capillary length λ of the working liquid

$$\lambda = \sqrt{\frac{\gamma}{\rho g}}, \tag{1}$$

where g is the gravitational acceleration and γ and ρ are the surface tension and mass density of the liquid, respectively. The tip of an externally-fed emitter must stick out above the free surface of the liquid reservoir to be able to operate. If the emitters are approximated as solid cylinders, then the height that the liquid meniscus will climb up their outside surface is given approximately by h_{climb}

$$h_{climb} = b \cdot \ln\left(\frac{2\lambda}{b}\right), \tag{2}$$

where b is the cylinder radius [27]. Therefore, the meniscus will climb a distance on the order of λ for b on the order of λ. For $b \ll \lambda$, the meniscus climbs a distance several times b. To be clear, h_{climb} is the height of the meniscus external to the emitter structure; liquid can rise higher than this by propagating through wicking structures on the emitter surface. In general, then, a safe design criterion is that the length of the emitter l_e be at least an order of magnitude larger than the width of the emitter. For surface tension to sustain flow against gravity, the wicking structures on the emitters must have a characteristic length on the order of λ or less. Smaller structures can wick to a higher elevation but generally exhibit slower dynamics than structures on the order of λ. The designs explored in this work include emitters a few millimeters long with sub-millimeter cross-sections that are covered with tens-of-microns-sized micropillar arrays as wicking structure.

The micropillar structure in the devices reported in this paper acts as a 'sponge', increasing the amount of liquid retained by the emitter when dipped into the working liquid [28]. The devices operate continuously and steadily for about a minute before running out of liquid. Therefore, the reported devices are compatible with cyclic replenishing of the liquid coating, either by a rotary drum like the approach used in some commercial electrospinning sources [29] or a piston-like movement that submerges the emitters between periods of emission. In an advanced version of the device the wicking structure would continuously and passively feed the emitter from a liquid reservoir, similar to reported externally-fed microfabricated multiplexed electrospray ionic liquid ion sources that use nanostructured black silicon [30] or plasma-enhanced chemical vapor deposited (PECVD) carbon nanotubes [31] as wicking media; however, the non-Newtonian nature and high viscosity of the liquids used in electrospinning requires a wicking structure with very different characteristic dimensions. We recently demonstrated an engineered

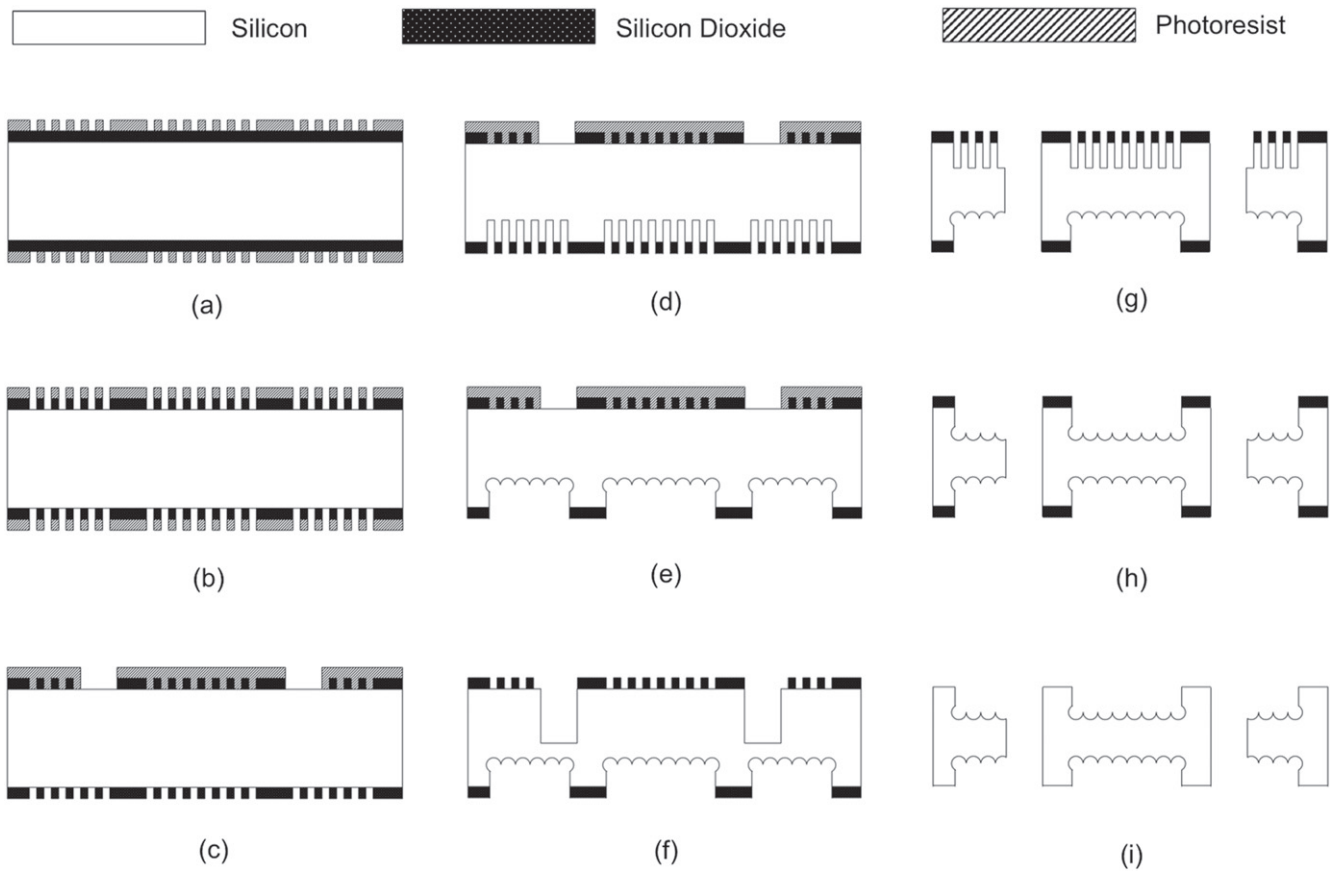

Figure 3. Schematic of process flow to fabricate the emitter blades. First, contact lithography is conducted on both sides of a single-crystal silicon wafer that is coated on both sides with 1 μm thick PECVD silicon oxide and 1 μm thick photoresist to transfer the micropillar pattern to the photoresist films (a); the features are then transferred to the oxide films using RIE (b). Next, the photoresist is stripped and a second lithography is done on the front surface of the wafer to transfer the outlines of the emitter blades to the oxide film using a 10 μm thick photoresist film (c). After that, the micropillar features are etched into the backside of the wafer using DRIE (d), and an isotropic RIE step etches away the dummy features of the micropillar pattern (e). The wafer is flipped over and mounted onto a quartz wafer using photoresist to allow for through-etching. The outline of the emitter blades is partially etched into the front surface of the wafer, and the photoresist film is stripped (f). Afterward, the micropillar features are etched into the front surface using DRIE (g), and an isotropic RIE step removes the dummy features from the micropillar array (h). At this point, the fabrication of the emitter blades is completed but they are still attached to the substrate with tethers. Finally, the emitter blades are extracted from the substrate by breaking with tweezers the tethers, an any remaining PECVD oxide coating is stripped using a BOE bath (i).

microstructured surface that wicks the liquids used for electrospinning across vertical surfaces for over 1 cm in vertical height and that can continuously feed electrospray emission [32], suggesting the feasibility of implementing an array of electrospinning emitters that is fed passively, externally, and continuously.

A microfabrication process flow was conceived to accommodate the hierarchical length scales of the proposed design. Linear (i.e., one-dimensional) arrays of millimeter-scale tall emitters with hundreds-of-microns tip diameter are monolithically patterned on a silicon wafer and micro-scale wicking features are patterned on its top and bottom surfaces. The emitter blade cutouts are then precisely assembled into a microfabricated slotted base to form planar (i.e., two-dimensional) emitter arrays, which are on the order of square centimeters in size. The design space included three different emitter spacings (1, 2, and 3 mm), two emitter-tip radii (125 and 250 μm), and as wicking structure an array of pillars with 65 μm width, 250 μm pitch, and 125 μm height. In all cases the emitters were 6 mm long. The fabrication of the blades (i.e., linear arrays of emitters with two-sided roughness) is shown in figure 3. The substrates used to make the blades are 500 μm thick, n-type single-crystal silicon wafers that are double-side-polished and coated with 0.5 μm of thermal oxide. First, a 1 μm thick PECVD silicon oxide film is deposited on both sides of the wafer; the wafer is then annealed for 1 h in nitrogen at 950 °C to improve the etch selectivity of the film. Next, contact lithography is done on both sides of the wafer to transfer the micropillar pattern to a 1 μm thick photoresist film (figure 3(a)); the pattern includes both the pillar features and dummy features to fill-in the space between the pillars to enforce vertical sidewalls of the etching. The features on the photoresist film are transferred to the oxide films using reactive-ion etching (RIE) (figure 3(b)). The photoresist is stripped and a second lithography is done on the front surface of the wafer to transfer the 'cookie-cut' features that outline the blades to a 10 μm thick photoresist film, and the exposed oxide is removed with RIE (figure 3(c)). The

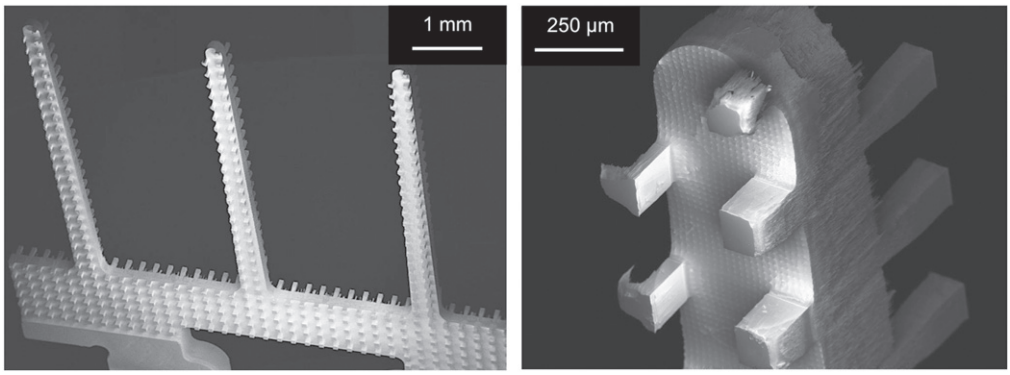

Figure 4. SEM images of a fabricated monolithic linear array of externally-fed emitters (left) and close-up of an emitter tip (right). The emitters are a few millimeters long and have sub-millimeter cross-sections. The top and bottom surfaces of the linear arrays are covered with arrays of tens-of-microns-sized micropillars, which serve as a wicking structure that retains liquid that eventually is electrohydrodynamically ejected by the emitter trips.

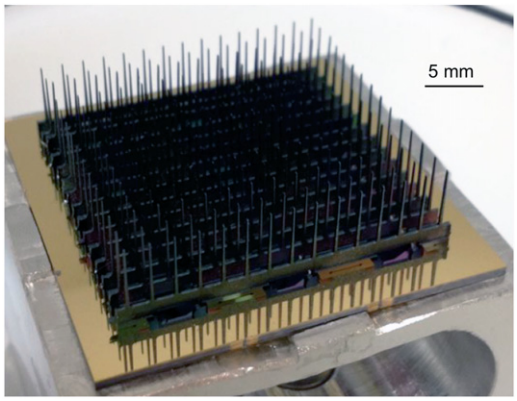

Figure 5. Image of an assembled planar array of 15×15 emitters with emitter density equal to 25 emitters cm^{-2}.

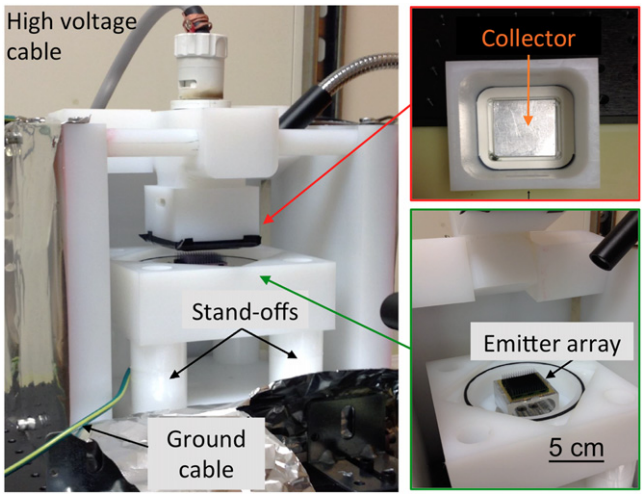

Figure 6. Experimental apparatus (left) with close-up detail of the collector electrode (top right) and emitter array installed in the apparatus (bottom right). The emitter array is installed on top of a metal base that is inside an open container. A flat collector electrode faces the emitter array, defining a constant separation between the emitter tips and the collector. To activate the array, the emitters are soaked in PEO solution and a bias voltage is applied between the metallic base and the collector electrode.

micropillar features and dummy features are etched into the backside of the wafer using DRIE (figure 3(d)), and an isotropic RIE step etches away the dummy features of the micropillar pattern (figure 3(e)). The wafer is flipped over and mounted onto a quartz wafer using photoresist to allow for through-etching. The outline of the blades is partially etched into the front surface of the wafer, and the photoresist film is stripped (figure 3(f)). Next, the micropillar features are etched into the front surface using DRIE (figure 3(g)), and an isotropic RIE step removes the dummy features (figure 3(h)); this etch finalizes the patterning of the outline of the blades, which are still attached to the substrate with tethers. Finally, the emitter blades are extracted by breaking with tweezers the tethers that hold the blades attached to the substrate, and any PECVD oxide coating on the blades is removed using a buffered oxide etch (BOE) bath (figure 3(i)).

SEM images of a fabricated emitter blade are shown in figure 4. Slotted plates that hold the emitter blades were fabricated using DRIE and contact lithography; the slots in the plate precisely match features in the emitter blades to assemble devices with precision on the order of tens of microns. Arrays with as many as 225 emitters (25 emitters cm^{-2}) (figure 5) and emitter densities as large as 100 emitters cm^{-2} (100 emitters) were assembled and characterized. To our knowledge, these are the largest and densest arrays comprised of fixed, precisely located emitters that have been used to electrospin nanofibers. An advanced version of the devices would include a proximal electrode grid where each emitter is surrounded by an aperture to lower the operational voltage. In that case, it is important to have the emitters well aligned to the grid; therefore, more precise methods of assembly of the blades could be used (e.g., microfabricated deflection springs that provide micron-level alignment with submicron repeatability [33, 34]).

Experimental procedure

The devices were tested in a diode configuration using a custom apparatus shown in figure 6. Most of the setup was made of ultra-high molecular weight polyethylene or

polyphenylene sulfide because of their high dielectric strength, machinability, and good mechanical properties. The apparatus included a liquid bath container that holds a metal base to affix the device that is tested, and a metal collector plate covered by an aluminum foil cut-out to both capture imprints and measure currents. The apparatus enforced constant separation between the collector and the emitter tips of the array; the separation can be varied by changing the spacers that hold the liquid bath container. The apparatus had a digital camera with a lens that allowed visual inspection of the emitters during the experiments. In the experiments, the emitter array was affixed to the metal base and a fixed amount of liquid was deposited over each emitter using a syringe. The liquid used was 4% (m/v) polyethylene oxide (PEO) in 2:3 ethanol/water. The liquid coated the emitters forming a thick layer, and any excess liquid dripped into the liquid bath container. The emitter array was grounded and the collector plate was biased at a high voltage using a Spellman Bertan 225-50R high voltage power supply that is PC controllable and can deliver up to 50 kV dc bias voltage. In a typical experiment, the voltage was ramped from zero to the chosen value at a constant rate and then held at that value for a specific time before ramping back down to zero. The constant-voltage time, which was set by trial and error to operate the device in steady state without running out of liquid, was typically on the order a minute. A software program recorded both the voltage and current traces at a sampling rate of roughly once every 700 ms. Each experiment was run multiple times to verify repeatability and collect thick imprints. After the series of runs, the foil was removed and placed overnight in a covered container in a nitrogen box so that any remaining solvent would evaporate. The foil was weighed to measure the mass production rate of the process, and the imprints were imaged with optical and scanning electron microscopes. The experiments were conducted in a room without direct sunlight, at a controlled ambient temperature of 20 °C and a relative humidity of 45% that were regulated by a cleanroom HVAC system.

Experimental results and discussions

With a separation distance between the emitter tips and the collector plate of 1 cm, uniform electrospinning across emitter arrays was observed, with each emitter generating an anchored, stable fiber. These experiments produced roughly uniform deposits on the collector that matched the distribution of the emitter array (figure 7), producing unwoven mats of nanofibers with average diameter equal to 250 nm when the separation between adjacent emitters was equal to at least 2 mm (figure 8). For a separation distance between the emitter tips and the collector plate of 2 and 3 cm, collector imprints were no longer comprised of a one-to-one matching array of dots; instead, deposition occurred uniformly over the area of the array creating one large patch, likely due to greater growth of the whipping instability as the fiber jet travels a longer distance to the collector. A summary of the mass flux rates measured in these experiments is shown in table 1. The

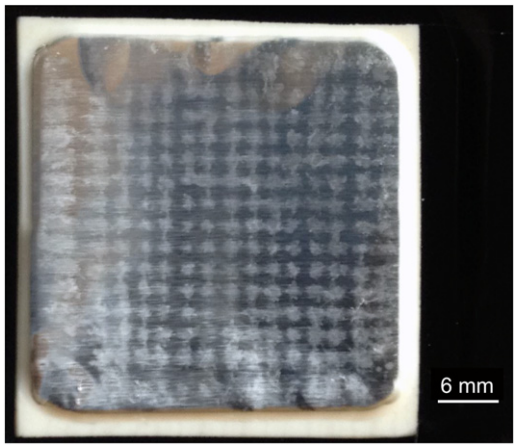

Figure 7. Collector imprint from a planar array of 225 emitters with 125 μm tip radius, with adjacent emitters spaced 2 mm apart.

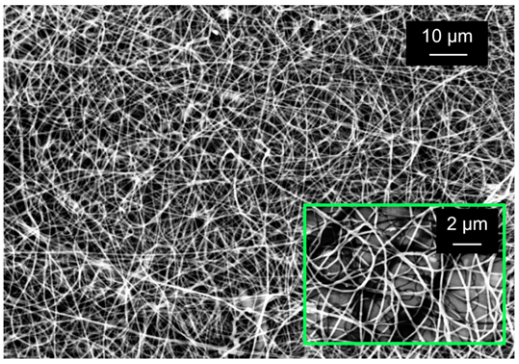

Figure 8. SEM image of an unwoven electrospun nanofiber mat and SEM close-up of the nanofibers.

largest arrays tested (225 emitters, 25 emitters cm^{-2}) produced a total mass flux of 82 ± 10.25 mg hr^{-1} m^{-2}, which is close to the 100 mg hr^{-1} m^{-2} flux produced by commercial free-surface electrospinning sources [29]; however, the microfabricated devices operated at 8.2 kV as opposed to the 30–100 kV typically used in commercial free-surface electrospinning sources, which represents over 72% in power consumption savings for the same nanofiber flux. The largest mass flux measured was 417 g hr^{-1} m^{-2} for a 4×4 array of emitters operated with an emitter tips-to-collector separation of 3 cm and a bias voltage of 25 kV—a fourfold increase in flux compared to leading commercial free-surface electrospinning sources. The data show greater mass throughput for arrays with more emitters when all other parameters are equal; this may seem trivial, but it is an important result as it suggests that the design can be scaled up without a loss of productivity. Arrays with the same emitter density operated with the same bias voltage and emitter tips-to-collector separation produce the same per-emitter mass flowrate. Also, arrays of the same size, emitter density, bias voltage, and separation distance between the emitter tips and the collector plate, but different in-plane tip radii, generate comparable per-emitter flow rates. This supports the notion that the field enhancement in each emitter is mostly caused by the sharp edge left by the DRIE processing. In addition, the data suggest that the bias

Table 1. Mass production rates of various emitter arrays.

Emitter array size	Bias voltage (kV)	Distance from emitter tips to collector plate (cm)	Separation between adjacent emitters (mm)	In-plane tip radius of curvature (μm)	Average mass flow rate per emitter (mg hr^{-1})	Average mass flux (g hr^{-1} m^{-2})
6 × 6	7.2	1	2	125	0.15 ± 0.05	37.5 ± 12.5
15 × 15	7.2	1	2	125	0.16 ± 0.04	40 ± 10
6 × 6	8.2	1	2	125	0.25 ± 0.05	62.5 ± 12.5
15 × 15	8.2	1	2	125	0.33 ± 0.04	82.5 ± 12.5
6 × 6	25	3	2	125	1.0 ± 0.33	250 ± 83
6 × 6	25	3	2	250	1.3 ± 0.1	325 ± 25
4 × 4	18	2	3	250	3.5 ± 0.5	389 ± 56
4 × 4	25	3	3	250	3.75 ± 0.75	417 ± 83

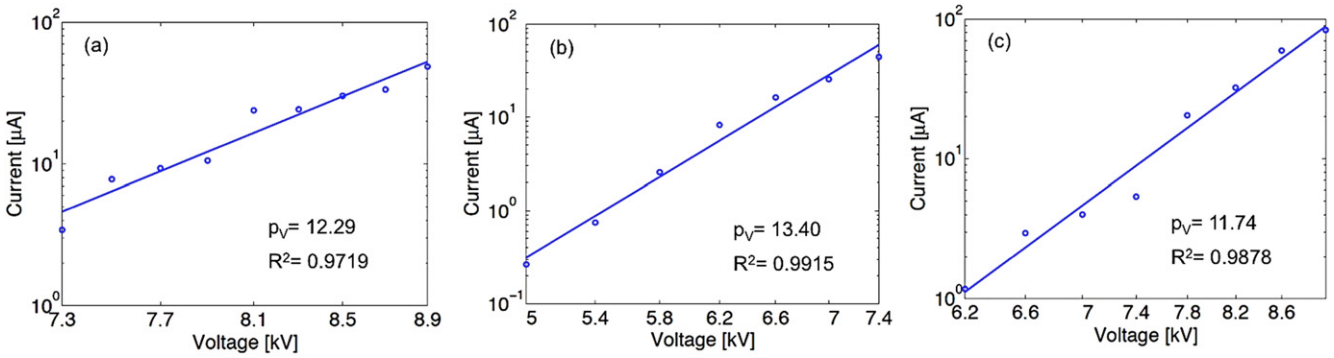

Figure 9. Average current versus bias voltage data with least-squares power law fits for various arrays for (a) 6 × 6 array with $R_{Tip} = 250$ μm, (b) 6 × 6 array with $R_{Tip} = 125$ μm, (c) 10 × 10 array with $R_{Tip} = 125$ μm; the coefficient of determination (R^2) for the fits is also given. In these experiments, the separation distance between the emitter tips and the collector is 1 cm and the emitter pitch is 2 mm.

voltage plays a major role in the per-emitter production of nanofibers, up to a point, as the electric field on the emitter tips can be increased only to a certain extent before arcing occurs [35]. Therefore, the largest array flux would be obtained by using devices with the largest per-emitter mass flow rate times the emitter density; in this case, the use of microfabrication techniques would still be beneficial to achieve monolithic manufacture of emitter blades with very sharp tips at a low cost. In a device with a proximal electrode grid it might be possible to decouple the per-emitter characteristics from the emitter density and achieve the largest flux from the devices with the largest emitter density.

Quantitative semi-empirical models for the emitted current from an electrospray emitter operating in the cone-jet mode have been reported [36–38]; however, the cone-jet mode produces droplets instead of fibers, and in most of these models the flowrate is an independent variable rather than a response of the system to some applied bias voltage. Electrospinning current I has been empirically modeled with a power law in the applied bias voltage V at fixed flow rates according to [39]

$$I = k_V V^{p_V}, \tag{3}$$

where k_V and p_V are experimental constants. We followed this modeling approach and the current versus bias voltage characteristics of the devices are shown in figure 9. The plots report the steady-state current (i.e., given the transients in bias voltage for a typical experiment, the current also has a transient ramp-up time, followed by a steady-state operation and a transient ramp-down time). For the arrays tested, the fitted exponent p_V falls between 11 and 14 with an average around 12; this value is much larger than the exponents reported for traditional needle electrospinning of the same polymer solution, which are around 3 [39], which evidences the greater field enhancement of the microfabricated emitters.

For some of the arrays tested at a separation distance between the emitter tips and the collector plate of 2 and 3 cm, total mass flux was greater than it was at 1 cm separation; this may seem counter-intuitive but makes sense if one considers how the emitter field enhancement varies across the array. The edge emitters produce higher field enhancement than interior emitters; therefore, they should be more productive at a given bias voltage. However, the difference in field enhancement between the two kinds of emitters increases the closer the array is to the collector. Since the maximum local electric field at the edge emitters is limited to the breakdown strength of the air, the average field felt across the array is greater with greater separation between the emitter tips and collector.

The arrays with 1 mm emitter spacing did not produce any fiber emission. Examination of the collector foil for all experiments using a 10 × 10 array of emitters spaced at 1 mm reveals small specks of polymer distributed quite uniformly within circular regions on the foil that lined up with the emitters (figure 10). The specks of polymer observed on the

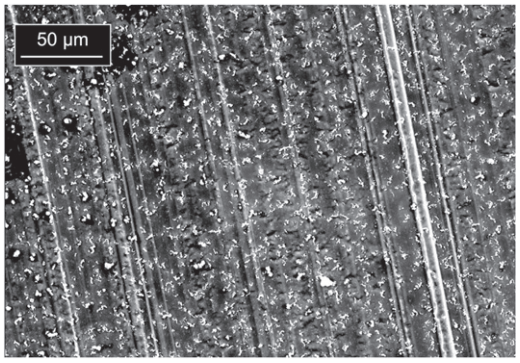

Figure 10. SEM close-up of imprint from an array of 100 emitters spaced 1 mm apart.

foil have diameters ranging primarily between 1 and 5 μm, with none larger than 10 μm. These deposits are probably the result of electrospray droplet emission, which is typically observed for less viscous conductive liquids. High viscosity liquids usually produce fibers in a strong electric field, but it is possible that a lack of sufficient liquid flow at the emitter tips resulted in droplet formation. Electrospray has been extensively studied and the minimum droplet radius $R_{\mathrm{drop,min}}$ has been shown to scale as

$$R_{\mathrm{drop,min}} = \left(\frac{\gamma \tau_{\mathrm{e}}^2}{8\rho}\right)^{\frac{1}{3}}, \tag{4}$$

where τ_{e} is the electrical relaxation time,

$$\tau_{\mathrm{e}} = \frac{\varepsilon_{\mathrm{r}}\varepsilon_{\mathrm{o}}}{\mathrm{K}} \tag{5}$$

where ε_{r}, ε_{o}, and K are the relative electrical permittivity of the liquid, the electrical permittivity of free space, and the electrical conductivity of the liquid, respectively [37]. Equation (4) predicts a minimum droplet diameter of about 0.5 μm for 4% (m/v) PEO in 2:3 ethanol/water ($\gamma = 0.04\ \mathrm{N\,m^{-1}}$, $\rho = 916\ \mathrm{kg\,m^{-3}}$, $K = 1.15\ \mathrm{mS\,m^{-1}}$; $\varepsilon_{\mathrm{r}} = 66.57$ [39]). If it is assumed that the specks were left behind by the evaporation of a droplet of the working liquid, this means the initially emitted droplet would have had a diameter approximately three times larger than the speck. Such droplets are above the 0.5 μm lower limit, suggesting that electrospray is occurring. Observations from imaging the collector imprints also indicate that electrospray likely occurred simultaneously with electrospinning during some of the fiber-producing tests. This would explain the observation, in some cases, of alternative polymer structures containing partially dissolved nanofibers. These structures were originally attributed to insufficient evaporation of solvent; however, previous experiments using the same hardware and working liquid had successfully spun clean, uniform fibers at the same working distances. Even though the original intention of the work was to explore novel hardware for nanofiber manufacture, the alternative polymer structures are interesting and potentially useful in their own right. For example, the electrospray process observed could be used to evenly disperse fine droplets of some viscous catalyst that would otherwise be difficult to generate [5].

Although emission from each emitter in an array was achieved at sufficiently large bias voltages, this does not necessarily mean that each emitter experienced the same field strength; in particular, the outer emitters are expected to experience larger fields than the inner emitters. Therefore, per-emitter emission might not be uniform across the array. For this reason, a grounded edge electrode was investigated on a 4 × 4 array of emitters with 3 mm spacing. Similar work with ring electrodes has demonstrated improved uniformity due to reduced field enhancement at the array edge [40]. The edge electrode was a conducting plate with a 15 mm by 15 mm square aperture. The geometric center of the area of the array and the aperture line up, defining a constant gap of about 3 mm around the array, which is also the emitter spacing for the arrays used in these tests. The edge electrode sat approximately 2 mm below the plane of the emitter tips and was grounded with the emitter array. The array was operated with separation distances between the emitter tips and the collector plate of 1 and 2 cm; imprints are shown in figure 11. The use of the ground electrode yields more uniform imprints on the collector, and extends the range of separation distances where an imprint for each emitter can be distinguished on the collector plate.

Identical emitter arrays can be tiled in such a way that they effectively create a single, mega array in which emitter-to-emitter spacing is uniform throughout. As discussed before, some deviation is to be expected between the output of an edge emitter and an internal emitter due to different field enhancement characteristics. However, the larger the array, the smaller the percentage of emitters that would be at the edge. For example, in an array with total area of 1 $\mathrm{m^2}$ and a 2 mm emitter spacing, less than 1% of the 250 000 emitters in the array are edge emitters. The majority of the emitters in the interior will experience very similar electric fields and, therefore, should exhibit similar mass throughput. In practical terms, the planar arrays of emitters are made from assembling monolithic linear arrays of emitters fabricated from single-crystal silicon wafers, which limits the maximum length of the array. In this work we used 6 inch wafers but there are 12 inch wafers commercially available and the semiconductor industry is working on producing 18 inch wafers in the near future. If we set at 75% of the wafer diameter the maximum length of the linear array we can make, it would imply a maximum length of 34.3 cm for the 18 inch substrates, in which 171 emitters spaced 2 mm or 114 emitters spaced 3 mm can be made. The size of the linear arrays would effectively limit the size of the planar arrays that could be tiled to make the mega arrays.

A pending issue of the technology is the demonstration of continuous nanofiber generation for arbitrarily long periods of time. The reported devices are compatible with cyclic replenishing of the liquid coating, either using a rotary drum like the one used in some commercial electrospinning sources, or a piston-like movement that submerges the emitters between periods of nanofiber emission. We recently demonstrated an engineered microstructured surface that wicks the

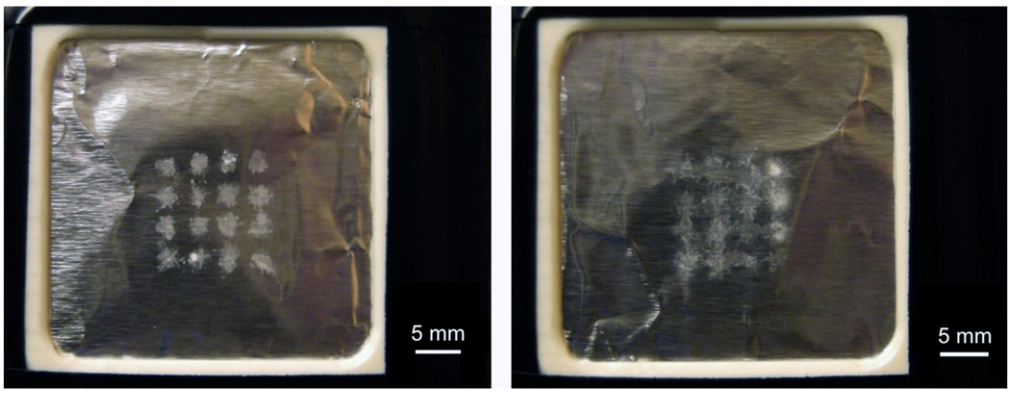

Figure 11. Collector imprints from a 4 × 4 emitter array with 3 mm emitter separation using an edge ground electrode: (left) for a 1 cm separation distance between the emitter tips and the collector plate, deposition is highly localized; (right) for a 2 cm separation distance between the emitter tips and the collector plate, deposition is less localized than at 1 cm but much more so than operating the device at the same separation distance but without the edge electrode.

liquids used for electrospinning across vertical surfaces for over 1 cm in vertical height and that was used to continuously feed electrospray emission [32]. This suggests the feasibility of implementing an array of electrospinning emitters that is fed externally, passively, and continuously.

Our experiments involved short run times with manual replenishment of the working liquid; in the experiments we did not see any evidence of liquid drying out before being ejected. However, a continuously operating system might face excessive solvent evaporation from the free surface of the externally-fed electrospinning system, which could cause drying out the working liquid before is emitted as nanofibers; a potential solution to this problem is continuously mixing new solvent into the liquid bath to compensate for the evaporated solvent. A continuously operating array may also saturate the surrounding air to the point where nanofiber production becomes severely limited, as the jet cannot dry before reaching the collector electrode. In such case, the arrays could be modified to incorporate channels delivering dry air to the fiber-emission zone, much like in gas-assisted electrospinning [41].

Conclusions

The design, microfabrication, and characterization of externally-fed emitter arrays for parallel nanomanufacturing via externally-fed electrohydrodynamic jetting was reported. Nanofiber generation from two-dimensional arrays with as many as 225 emitters spaced as close as 2 mm apart was demonstrated. Increasing the size of the array while keeping the emitter density constant increases the total throughput, which suggests that the production method studied here can be scaled up without loss in productivity. Arrays with the same emitter density, operated with the same bias voltage and distance between emitter tips and the collector plate, produced the same per-emitter mass flowrate. Also, arrays of the same size, emitter density, bias voltage, and distance between emitter tips and the collector plate, but different in-plane tip radii, generated comparable per-emitter flow rates, supporting the notion that the field enhancement in the emitter is mostly caused by the sharp edge left by the DRIE processing. In addition, the data suggest that the bias voltage plays a major role in the per-emitter production of nanofibers, up to a point, beyond which further increases in the electric field result in arcing. The largest array flux would be obtained from devices with the largest per-emitter mass flow rate times the emitter density. The largest mass flux measured was on the order of 417 $g\,hr^{-1}\,m^{-2}$ for a bias voltage of 25 kV; this is several times the production rate of the leading, commercial free-surface electrospinning technology. Production rates as high as 80 $g\,hr^{-1}\,m^{-2}$ were measured for bias voltages as low as 8.2 kV, highlighting the benefit of using electric field enhancing structures for lowering the power requirements. While operating the emitter arrays with a separation distance between emitter tips and the collector plate of 1 cm, we were able to spin nanofibers forming deposits from each emitter in the array that are approximately uniform, suggesting the possibility to use the devices as a 'dot matrix' printer head to create deposits of nanofibers at specific locations on a collector substrate. The inclusion of a grounded electrode that lowers the electric field experienced by emitters at the edge of the array allowed for a larger emitter tips-to-collector separation while still being able to distinguish an individual imprint for each emitter of the array. Nanofibers were not observed for any array with emitter spacing of 1 mm; the emission appeared to be made of droplets. Finally, the current versus voltage characteristics were mapped by a least-squares power fit, in agreement with reports in the literature.

Acknowledgments

The microfabrication of the devices was completed using the facilities at the Microsystems Technology Laboratories (MTL) of the Massachusetts Institute of Technology. This work was supported in part by the Defense Advanced Research Projects Agency/Microsystems Technology Office under contract W31P4Q-11-1-0007 (program manager Jack Judy). Any opinions, findings, and conclusions or

recommendations expressed in this publication are those of the authors and do not necessarily reflect the views of the US Government and therefore, no official endorsement of the US Government should be inferred.

References

[1] Taylor G 1964 Disintegration of water drops in electric field *Proc. R. Soc.* **280** 383–97

[2] Garoz D, Bueno C, Larriba C, Castro S, Romero-Sanz J, Fernandez de la Mora J, Yoshida Y and Saito G 2007 Taylor cones of ionic liquids from capillary tubes as sources of pure ions: the role of surface tension and electrical conductivity *J. Appl. Phys.* **102** 064913

[3] Cloupeau M and Prunet-Foch B 1994 Electrohydrodynamic spraying functioning modes: a critical review *J. Aerosol Sci.* **25** 1021–36

[4] Bhardwaj N and Kundu S C 2010 Electrospinning: a fascinating fiber fabrication technique *Biotech. Adv.* **28** 325–47

[5] Jaworek A 2007 Electrospray droplet sources for thin film deposition *J. Mater. Sci.* **42** 266–97

[6] Grenier A and Wendorff J 2007 Electrospinning: a fascinating method for the preparation of ultrathin fibers *Angew. Chem., Int. Ed. Engl.* **46** 5670–703

[7] Thavasi V, Singh G and Ramakrishna R 2008 Electrospun nanofibers in energy and environmental applications *Energy Environ. Sci.* **1** 205–21

[8] Sill T J and von Recum H A 2008 Electrospinning: applications in drug delivery and tissue engineering *Biomaterials* **29** 1989–2006

[9] Thoppey N M, Bochinski J R, Clarke L I and Gorga R E 2010 Unconfined electrospun into high quality nanofibers from a plate edge *Polymer* **51** 4928–36

[10] Nakajima T 1994 *Advanced Fiber Spinning Technology* (Amsterdam: Elsevier)

[11] Thompson P A 1972 *Compressible Fluid Dynamics* (New York: McGraw-Hill)

[12] Zhou F-L, Gong R-H and Porat I 2009 Mass production of nanofiber assemblies by electrospinning *Polym. Int.* **58** 331–42

[13] Srinivasan G and Reneker D H 1995 Structure and morphology of small diameter electrospun aramid fibers *Polym. Int.* **36** 195–201

[14] Yarin A and Zussman E 2004 Upward needleless electrospinning of multiple nanofibers *Polymer* **45** 2977–80

[15] Lukas D, Sarkar A and Pokorny P 2008 Self-organization of jets in electrospinning from free liquid surface: a generalized approach *J. Appl. Phys.* **103** 084309

[16] Thoppey N, Bochinski J, Clarke L and Gorga R 2011 Edge electrospinning for high throughput production of quality nanofibers *Nanotechnology* **22** 345301

[17] Wang X, Niu H, Lin T and Wang X 2009 Needleless electrospinning of nanofibers with a conical wire coil *Polymer Eng. Sci.* **49** 1582–6

[18] Petrik S and Maly M 2009 Production nozzle-less electrospinning nanofiber technology *MRS Fall Meeting* **vol 1240** WW03-07

[19] Velásquez–García L F, Akinwande A I and Martínez–Sánchez M 2006 A micro-fabricated linear array of electrospray emitters for thruster applications *J. Microelectromech. Syst.* **15** 1260–71

[20] Krpoun R and Shea H R 2009 Integrated out-of-plane nanoelectrospray thruster arrays for spacecraft propulsion *J. Micromech. Microeng.* **19** 045019

[21] Gassend B, Velásquez-García L F, Akinwande A I and Martinez-Sanchez M 2009 A microfabricated planar electrospray array ionic liquid ion source with integrated extractor *J. Microelectromech. Syst.* **18** 679–6694

[22] Srivastava Y, Marquez M and Thorsen T 2007 Multijet electrospinning of conducting nanofibers from microuidic manifolds *J. Appl. Polymer Sci.* **106** 3171–8

[23] Pan Y, Huang Y, Bu N and Yin Z 2013 Fabrication of Si-nozzles for parallel mechano-electrospinning direct writing *J. Phys. D: Appl. Phys.* **46** 255301

[24] Chang C, Limkrailassiri K and Lin L 2008 Continuous near-field electrospinning for large area deposition of orderly nanofiber patterns *Appl. Phys. Lett.* **93** 123111

[25] Fuh Y-K, Chen S-Y and Ye J-C 2013 Massively parallel aligned microfibers-based harvester deposited via *in situ* oriented poled near-field electrospinning *Appl. Phys. Lett.* **103** 033114

[26] Chen K-S, Ayon A A, Zhang X and Spearing M 2002 Effect of process parameters on the surface morphology and mechanical performance of silicon structures after deep reactive ion etching (DRIE) *J. Microelectromech. Syst.* **11** 264–75

[27] De Gennes P-G, Brochard-Wyart F and Quere D 2004 *Capillarity and Wetting Phenomena: Drops, Bubbles, Pearls, Waves* (Berlin: Springer)

[28] Seiwert J, Clanet C and Quéré D 2011 Coating of a textured solid *J. Fluid Mech.* **669** 55–63

[29] Kurečič M and Smole M S 2013 Electrospinning: nanofibre production method *Tekstilec* **56** 4–12

[30] Velásquez-García L F, Akinwande A I and Martínez–Sánchez M 2006 A planar array of micro-fabricated electrospray emitters for thruster applications *J. Microelectromech. Syst.* **15** 1272–80

[31] Hill F A, Heubel E V, Ponce de Leon P and Velásquez-García L F 2014 High-throughput ionic liquid ion sources using arrays of microfabricated electrospray emitters with integrated extractor grid and carbon nanotube flow control structures *J. Microelectromech. Syst.* **23** 1237–48

[32] Ponce de Leon P and Velásquez-García L F Optimization of capillary flow through open-microchannel and open-micropillar arrays in preparation

[33] Velásquez-García L F, Akinwande A I and Martínez-Sánchez M 2007 Precision hand assembly of MEMS subsystems using DRIE-patterned deflection spring structures: an example of an out-of-plane substrate assembly *J. Microelectromech. Syst.* **16** 598–612

[34] Gassend B, Velásquez-García L F and Akinwande A I 2009 Precision in-plane hand assembly of bulk-microfabricated components for high voltage MEMS arrays applications *J. Microelectromech. Syst.* **18** 332–326

[35] Johnson M J, Tirumala R and Go D B 2015 Analysis of geometric scaling of miniature, multi-electrode assisted corona discharges for ionic wind generation *J. Electrostat.* **74** 8–14

[36] Fernandez de la Mora J and Loscertales I G 1994 The current emitted by highly conducting Taylor cones *J. Fluid Mech.* **260** 155–84

[37] Gañan-Calvo A M, Davila J and Barrero A 1997 Current and droplet size in the electrospraying of liquids Scaling laws *J. Aerosol Sci.* **28** 249–75

[38] Smith K, Alexander M and Stark J 2006 Voltage effects on the volumetric flow rate in cone-jet mode electrospraying *J. Appl. Phys.* **99** 064909

[39] Theron S, Zussman E and Yarin A 2004 Experimental investigation of the governing parameters in the electrospinning of polymer solutions *Polymer* **45** 2017–30

[40] Yang Y, Jia Z, Li Q, Hou L, Liu J, Wang L, Guan Z and Zahn M 2010 A shield ring enhanced equilateral hexagon distributed multi-needle electrospinning spinneret *IEEE Trans. Dielectr. Electr. Insul.* **17** 1592–601

[41] Zhmayev E, Daehwan C and Joo Y L 2010 Nanofibers from gas-assisted polymer melt electrospinning *Polymer* **51** 4140–4